Science & Technology Development Journal – Engineering and Technology, 4(3):1079-1092

Open Access Full Text Article

Research Article

Design of low cost-remote eye tracker using Pupil Center-Corneal Reflection technique

Phu Do Tuong, Linh Huynh Quang, Dang Le Cao, Tin Tran Trung*

ABSTRACT

The eye tracker is used in many fields such as education, marketing, psychology, medicine, among others. However, commercial devices are costly, spanning from a few hundred to several thousand dollars. Therefore, an inexpensive-monocular-remote (IMR) eye tracker is developed for education and research, which implements the Pupil-Center-Corneal-Reflection technique. The IMR device consists of a low-cost camera with a near-IR pass filter that captures subject's eye images, a moderate-cost computer that processes these images, as well as two near-IR light sources that create glints and illuminate the eye. The pupil detection algorithm is developed by combining the advantages of two recent algorithms, named BORE and PDIF, and gaze points are estimated from pupil-glints vectors via a fourth-order polynomial. An experimental evaluation is conducted concurrently on the research eye tracker IMR at the operating frequency of 30 Hz and the commercial-high-end-head-free device VT3 Mini at 60 Hz, in a challenge condition: subjects sit down near a window, and some of them wear glasses. Also, their heads are placed on a fixed chin rest, and the data is acquired when both devices successfully estimate gaze points. The experimental results in 11 sample data, obtained from 7 subjects, show that the overall ratio of the number of filtered/raw samples and raw/idea samples are 88.92% and 98.63% in order. Whereas the overall precision of the IMR eye tracker is nearly equal to that of the VT3 Mini device (0.57 degrees and 0.54 degrees, respectively), the overall accuracy of the proposed eye tracker is better than that of the commercial device (1.04 degrees and 1.34 degrees, respectively). Regarding eye safety, the radiant power and the burn-hazard-weighted radiance of the proposed device are much smaller than their limitations, according to IEC 62471. With these results, the IMR eye tracker is appropriate for education and needs to be improved in terms of data validation to satisfy the research purpose.

Key words: Eye tracker, gaze estimation, low cost, Pupil Center-Corneal Reflection technique, pupil center detection

Department of Biomedical Engineering, the Faculty of Applied Science, Ho Chi Minh City University of Technology, VNU-HCM, Vietnam

Correspondence

Tin Tran Trung, Department of Biomedical Engineering, the Faculty of Applied Science, Ho Chi Minh City University of Technology, VNU-HCM, Vietnam

Email: trtrtin@hcmut.edu.vn

History

- Received: 03-06-2021
- Accepted: 30-8-2021
- Published: 11-9-2021

DOI : 10.32508/stdjet.v4i3.856

Check for updates

INTRODUCTION

Inexpensive-commercial eye trackers such as the Tobii 4C, the Tobii Eye Tracker 5, the Eye Tribe Tracker, and the Pupil Labs are commonly used in many fields of research [1,2]. However, some of these devices suffer from a moderate accuracy of nearly 2 degrees and a significant lack of frame rates [1]. In addition, the reported accuracy could be calculated from the optimized data of the calibration process and could be the standard deviation rather than the average value [1,3].

Currently, there are two gaze estimation methods, named Feature-based and Appearance-based [4]. Whereas the former uses extracted eye features, the latter treats whole eye images as its inputs. The Feature-based consists of three approaches: 3D-model-based, Cross-ratio-based, and Regression-based [4]. The 3D-model-based models the visual axis and the object, and the gaze point is their intersection. The Cross-ratio-based is based on the geometry property under perspective. In the Regression-based, eye features are mapped on gaze points via a regression function [4,5]. In [6], this function is built based on compensating second-order effects rather than mathematically fitting. The Feature-based method commonly uses the Pupil Center-Corneal Reflection (PCCR) technique, where glints are used as reference points, and the eye movement is represented by the pupil-glints vector.

Two pupil detection algorithms, named BORE and PDIF, are developed for remote eye trackers and various light conditions, respectively [1,7]. The PDIF algorithm implements morphology operations, which are ellipse kernels in different sizes, to remove corneal reflections and noises, maintain pupil's shape and position, and increase its diameter [7]. One of the limitations of this algorithm is that the pupil center is determined manually [7]. The BORE algorithm is based on the oriented edge optimization equation [8]. Because this algorithm is based on gradient values, glints inside the pupil area affect the estimation of the pupil

Cite this article : Tuong P D, Quang L H, Cao D L, Trung T T. **Design of low cost-remote eye tracker using Pupil Center-Corneal Reflection technique**. *Sci. Tech. Dev. J. – Engineering and Technology;* 4(3):1079-1092.

center.

Because a glint is much smaller than a pupil, or free head movements are required, high resolution cameras are typically used for commercial-remote eye trackers, despite their high cost. For example, the free head device VT3 Mini has an image resolution of 2048x1080. High resolution eye images can be captured by a zoom lens and a low-resolution camera in a narrow field of view (like the ISCAN device). This solution is effective in designing a low cost-monocular eye tracker and lowering computational costs in image processing (see Pupil-glints dection section). In addition, the VT3 Mini uses a built-in FPGA to ensure its performance whereas low-cost devices such as the Tobii 4C, the Tobii Eye Tracker 5, the Eye Tribe Tracker, and the Pupil Labs utilize user's computers. This device costs more than 3500 USD in 2019 and operates at the default frequency of 60 Hz.

This study addresses the design of an inexpensive-remote-monocular (IMR) eye tracker, including hardware and software, with the target accuracy of 1 degree at 30 frames per second. Regarding the hardware, a low-cost VGA image sensor and a zoom lens are used to capture high resolution eye images, as well as a moderate-cost computer is utilized to process these images. In terms of software, free-cost libraries and software are implemented to obtain and process eye images, as well as design the user interface. To operate the IMR system in real-world conditions, a novel pupil detection algorithm is developed by combining the advantages of the BORE and the PDIF algorithm. The next section describes the IMR system and methods, consisting of pupil-glint detection, gaze estimation, and evaluation. Results section shows evaluation results, including the validation of raw and filtered data, as well as the accuracies and precision of both devices. These results are discussed in Discussion section. Finally, conclusions are provided in Conclusion section.

MATERIALS-METHODS

Descriptions of the IMR system

Gaze points are estimated by the Regression-based method and the PCCR technique. Firstly, eye images are captured with a camera. Secondly, for each eye image, the centers of pupil and corneal reflections are determined. Thirdly, a calibration matrix is calculated from pupil-glints vectors and stimulus points in the calibration process. This process is skipped if the matrix is estimated successfully. Finally, gaze points are estimated from these vectors, using the calibration matrix.

Hardware

The system consists of an eye tracker that illuminates the eye and captures eye images, a 19-inch monitor (E1913Sf, the pixel pitch equals 0.294 mm) that represents visual displays, and a chin rest that fixates the subject's head (Figure 1). The software runs on an Intel i5-4200U-1.6 GHz-4.0 GB RAM computer.

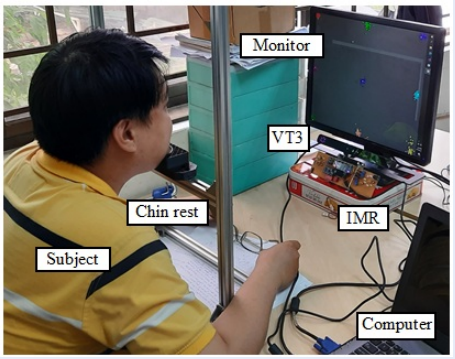

Figure 1: The VT3 Mini eye tracker and the IMR system.

a. The IMR eye tracker

The eye tracker includes a PS3 camera with a near-IR pass filter that captures subject's eye images, and two near-IR light sources that create glints and illuminate the eye (Figure 2).

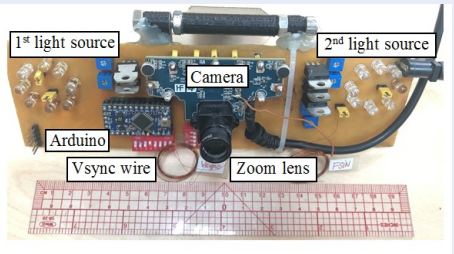

Figure 2: The IMR eye tracker.

The PS3's image sensor Omnivision OV7720 is a low-cost image sensor with a maximum operating frequency of 60 fps at VGA resolution and 187 fps at QVGA resolution, making it suitable for tracking fast eye movements such as saccades (10^o saccade takes 50 milliseconds). An 850 nm IR pass filter is utilized to eliminate visible light sources, which could cause unexpected glints, and an IR pass zoom lens with 25 mm of focal length that zooms the eye region.

2 near-IR light sources, each with 8 TSHG6410 LEDs at 850 nm wavelength are arranged in a circular shape

because the circle has the largest area compared to other figures, which have the same perimeter (the same number of LEDs). This solution is effective in creating large glints whose centers are the inputs of the gaze estimation algorithm (see Gaze estimation section). LEDs are supplied by a current source using LM317 as a current limiter at the current of 20 mA. Strobing lights, controlled by the switching MOSFET IRLML0030TRPbF and the Arduino via the Vsync signal, eliminate rolling shutter effects[9]. The emission power and the burn-hazard weighted-radiance are calculated and compared with standard limitation's IEC 62471.

The array of 16 LEDs TSHG6410 operates in the pulse mode, the duty cycle D = 0.5, the pulse time t_{pulse} = 0.017s, at the forward current I_F = 20mA, the minimum distance to user is 60 cm, the virtual source diameter D_{LED} = 2.1 mm the wavelength λ = 850 nm, and the exposure time is greater than 1000s. From the datasheet, the radiant power Φ_{chip} = 55 mW, the radiant intensity I_{LED} = 90 mW/sr, and I_{LED} (T = 25oC, IF = 20mA) = 16 x 20 mW = 0.32 W/sr.

The cornea hazard:

$$E = \frac{I}{d^2} = \frac{D_{chip}^2}{D_{LED}^2} = \frac{I_{chip}}{I_{LED}} = \frac{\phi_{chip}}{\pi \times I_{LED}} \tag{2}$$

$$D_{chip} = \sqrt{\frac{\phi_{chip} \times D_{LED}^2}{\pi \times I_{LED}}} = \sqrt{\frac{55mW \times (2.1mm)^2}{\pi \times 90mW/sr}} = 0.926mm \tag{3}$$

Where A_{chip} and A_{LED} are the active and the virtual area of the light source, respectively. The angular subtense α and the effective angular subtense α_{eff}:

$$\alpha = \frac{D_{chip}}{200} = \frac{0.926mm}{200mm} = 0.00463rad \tag{4}$$

$$\alpha_{eff}\left(t_{pulse} = 0.017s\right) = 0.0017rad \tag{5}$$

$$\alpha_{eff}\left(t_{pulse} = 1000s\right) = 0.011rad \tag{6}$$

The emission limit for the burn hazard weighted radiance EL_R and the emission limit for the burn-hazard-weighted radiance for low visible stimulus EL_{IR}:

$$EL_R = \frac{50000}{\alpha_{eff} \times t^{0.25}} = \frac{50000}{(0.0017rad) \times (0.017s)^{0.25}} = 81.45 \times 10^3 \frac{mW}{mm^2 \times sr} \tag{7}$$

$$L_R = \frac{R(\lambda) \times I_{LED}}{D_{chip}^2} = \frac{0.5 \times (320mW/sr)}{(0.926mm^2)} = 186.59 \frac{mW}{mm^2 \times sr} \tag{8}$$

The burn-hazard-weighting function:

$$R(\lambda) = 10^{\frac{700-\lambda}{500}} = 10^{\frac{700-850}{500}} = 0.5 \tag{9}$$

The burn-hazard-weighted radiance L_R and the burn-hazard-weighted radiance L_{IR} for low visible stimulus:

$$L_R = \frac{R(\lambda) \times I_{LED}}{D_{chip}^2} = \frac{0.5 \times (320mW/sr)}{(0.926mm)^2} = 186.59 \frac{mW}{mm^2 \times sr} \tag{10}$$

$$L_{IR} = \frac{R(\lambda) \times I_{LED} \times D}{D_{chip}^2} = \frac{0.5 \times (320mW/sr) \times 0.5}{(0.926mm)^2} = 93.3 \frac{mW}{mm^2 \times sr} \tag{11}$$

Because both the L_R and the L_{IR} are much smaller than their limitations (EL_R and EL_{IR}, respectively), the proposed system is appropriate for all users. In addition, if the total reflection occurs on the corneal surface, the retinal hazard is eliminated, as well as glints with high pixel values, which are useful for detection, are obtained (see Pupil-glints detection section).

b. The chin rest

The gaze estimation method (see Gaze estimation section) requires a chin rest to fixate the subject's head. In addition, it is used to evaluate the eye tracker's accuracy and precision (see Evaluation method section). A 30x30x70 cm chin rest, made of the aluminum and the PLA plastic, can be adjusted in vertical and horizontal dimensions. Edges are rubbed or designed in curved shapes for safety purposes.

Software

The software consists of four windows, corresponding to four stages: image acquisition, calibration, gaze estimation, evaluation. The software is written in C++, using Visual Studio Community 2017. Additional libraries and software are listed in Table 1.

Figure 3 shows the user interface of the image acquisition process, consisting of five subregions: the scaled image of the IMR device, the estimated pupil center (the plus marker), and the estimated glint centers (cross makers) (1); the scaled image of the VT3 Mini device, the marked pupil (the plus marker) and glint centers (cross makers) (2); the user interface of camera parameters and the image processing (3); the pupil region of interest when morphology operations are implemented (4); and the glint region of interest

Table 1: Additional libraries and their functions.

Libraries and software's name	Function
Libusb ofxPS3EyeGrabber	To communicate with the IMR eye tracker.
OpenCV The compiled library of the BORE algorithm	To process images of the IMR device.
QuickLink API	To communicate with the VT3 Mini eye tracker.
openFrameworks	To create the user interface.
Octave	To analyze raw data.

Figure 3: The image acquisition window.

when the binary threshold is applied (5). The pupil-glints detection algorithm is illustrated in Pupil-glints detection section.

The stimulus points of the calibration and the evaluation process are described in Gaze estimation and Evaluation method section, respectively. In the calibration, if the IMR calibration matrix is estimated successfully from pupil-glint vectors and stimulus points, these vectors are applied again to the matrix to estimate gaze points, which are displayed on the monitor. In the gaze estimation stage, estimated gaze points of both eye trackers are displayed on the monitor in real time. Static or dynamic stimuli can be added because the user interface is transparent (as Figure 1 and Figure 3). In the evaluation stage, evaluation points are displayed at the end of this process (Figure 1).

Methods

Pupil-glints detection

There are two approaches whose validation depends on the success of the pupil detection in the previous frame. In Figure 4, the blue, red, and black arrows present the flow paths of approach 1, approach 2, and both, respectively. Because Haar Cascade Classifiers are costly, approach 1 is only used in the case of an unknown pupil center in the previous frame. In addition, default Cascade Classifiers for eye detection, which are available on OpenCV, sometimes detect unexpected regions such as eyebrows or nostrils. Therefore, eye regions are double-checked, which are based on the fact that glints only form on opening eyes.

In both approaches, two glints are detected in the region of 48x48 pixels. This solution is effective in lowering the computational cost and eliminating glints created by unexpected light sources (they usually appear in subjects wearing glasses as shown in Figure 3). Whereas the pupil region of interest is only 48x48 pixels in approach 2, that in approach 1 is much larger because it equals the eye region. To lower the cost of the pupil detection, Benedikt Hosp et al. use three light sources arranged in a specific order as markers to set the pupil region of interest [1]. Alternatively, Świrski et al. designs a customized Haar-like feature to detect the pupil in the eye region [10]. To meet the compatibility with VT3's light sources (see Evaluation method section) and the low-cost achievement, the IMR system uses two light sources (see Pupil-glints detection section). Regarding lowering the cost of the BORE's gradient calculation, the proposed algorithm uses morphology operations to remove glints and to smooth the pupil region. In addition, these operations also reduce the size of the pupil when large glint regions are captured by the zoom lens.

Gaze estimation

a. Transfer function

In this study, the Regression-based gaze estimation is used via the PCCR technique. The mapping between gaze point G(g_x, g_y) and the pupil center-glints vector V(x,y) is presented by a fourth-order polynomial [6]:

$$\begin{aligned} g_x &= a_0 + a_1x + a_2y + a_3xy + a_4x^2 \\ &\quad + a_5y^2 + a_6x^2y + a_7xy^2 + a_8x^2y^2 \\ g_y &= b_0 + b_1x + b_2y + b_3xy + b_4x^2 \\ &\quad + b_5y^2 + b_6x^2y + b_7xy^2 + b_8x^2y^2 \end{aligned} \quad (12)$$

With a_0, a_1, a_2, a_3, a_4, a_5, a_6, a_7, a_8, b_0, b_1, b_2, b_3, b_4, b_5, b_6, b_7, b_8 are calibration parameters, calculated in the calibration process. (12) has 18 unknowns, so 9 known gaze points and 9 pupil center-glints vectors are needed to solve this problem. The third and fourth terms are added for high-order compensation at corners whereas remaining terms are used for uniaxial, crosstalk, and corner corrections.

The calibration process is set as Figure 1. Subjects are asked to fixate their heads on the chin rest and focus on 9 calibration points displayed sequentially. To attract the subject's attention and allow them to have time for preparation, some animations are implemented. Firstly, a gray circle with a decreasing diameter is displayed in 0.7 seconds. Subjects can determine this animation when they focus on other points because the edge of the retina is sensitive to the direction of movements [11]. Secondly, a green circle, whose center has a small white circle, is displayed in 0.3 seconds. It allows subjects to prepare and be familiar with the position of the calibration point. Thirdly, a calibration point, which is a red circle with a small white circle at the center, is shown in 1.5 seconds. Finally, a green circle, whose center has a small white circle, is displayed in 2.0 seconds for relaxing.

For each calibration point, approximately 45 eye images (in 1.5 seconds) are captured, and the centers of pupils and glints are estimated (see Pupil-glints detection section). Next, the mean pupil center L is calculated. Similarly, the mean of the centers of the left glints (M) and the right glints (N) are computed. The mean glint center O is the mean value between M and N. Then, the pupil-glint vector is calculated from L and O. Finally, 9 pupil-glint vectors and their corresponding calibration points are used to estimate calibration parameters. The calibration procedure is conducted only once for each subject.

b. Spatial denoising

Estimated gaze points, which are outside the operating window [0, 0, 1200, 1024], are considered as noises and eliminated [12].

Evaluation method

Estimated gaze points of the IMR eye tracker are compared to those obtained simultaneously by a commercial-high-end device VT3 Mini. Whereas the IMR eye tracker estimates gaze points from the subject's right eye, the VT3 Mini device estimates those from both eye images. Measurements are conducted on 7 subjects with 11 samples, and 4 of them have no sight corrections. Because both eye trackers utilize two 850nm light sources to create glints, and the performance of the reference device has to be maintained, only light sources of the VT3 Mini are valid.

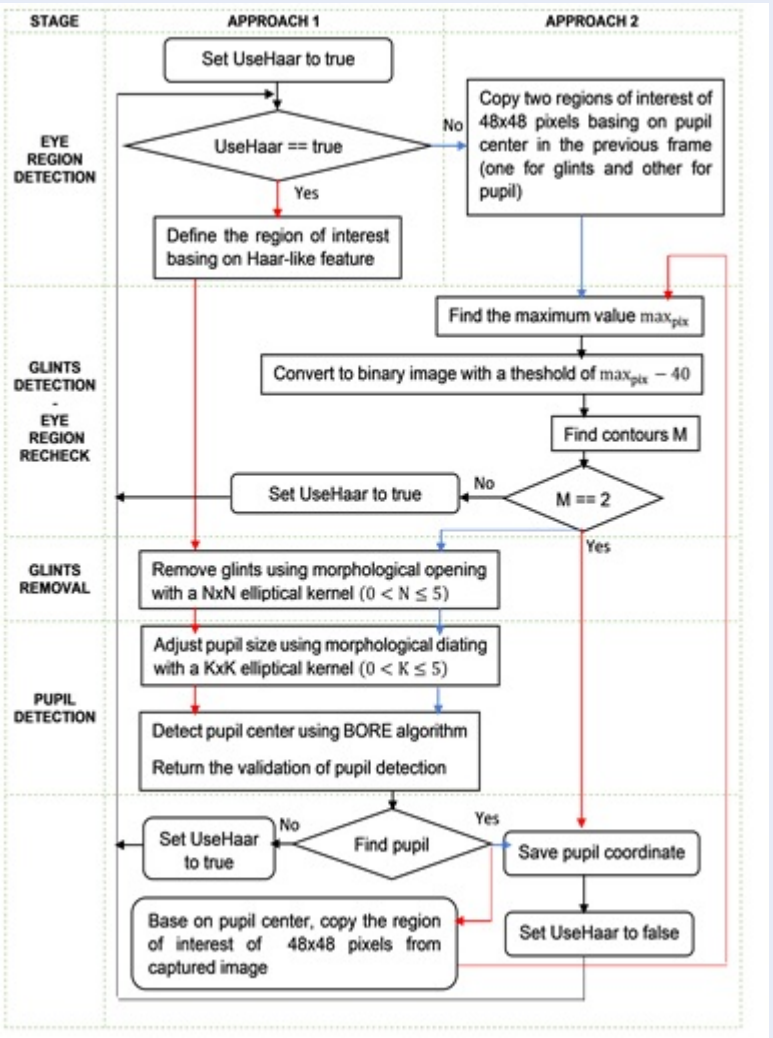

Figure 4: The flowchart of the proposed pupil-glints detection algorithm. The red, blue and black arrows present the flow paths of approach 1, approach 2, and both, respectively.

Because the VT3 Mini uses a built-in FPGA to do the whole process, a single thread for capturing and processing is used to simplify the programming. To ensure eye images are captured by both devices simultaneously, their capturing functions are called nearly. The two other threads for visual displays and waiting for GUI's changes are supported by openFrameworks. Because the VT3 Mini's producer claims it can operate outdoors and near windows, the performances of both eye trackers are tested in case they are put near a window (Figure 1).

The evaluation process is set as Figure 1. Firstly, subjects are asked to fix their heads on the chin rest and put their eyes at point $P\left(0, \frac{1}{3}H, 600\right)$ (the origin is the screen center, H is the vertical dimension of the monitor, unit in mm) as the producer's recommendation. The lens of the IMR device is adjusted to have high resolution images at the point P. The gain, the exposure and the kernel size of erosion operation, and the kernel size of dilation operation of the proposed device are 136, 3, 5 and 1, respectively.

Second, the calibration process of both devices is performed simultaneously. The position, time and the automatic recalibration for each point are decided by the VT3 Mini device. Animations, displayed for each point, are illustrated in Transfer function section.

Third, if the calibration matrix is estimated successfully, the evaluation process is validated. In this process, 9 evaluation points (1160,984), (600,984), (40,984), (40,512), (600,512), (1160,512), (1160,40), (600,40), and (40,40) are displayed in order. Animations, displayed for each point, are illustrated in Soft-

ware section. The raw data is obtained in case gaze points are estimated successfully by both devices. To be consistent with this condition, filtered points of both devices are collected in which the corresponding raw points are not outside the operating window.

Finally, the sample data is analyzed on GNU Octave, including the precision-accuracy calculation and the validation of filtered-raw data.

a. Precision and accuracy

The accuracy A and precision P of each eye tracker, corresponding to each subject, are calculated by (13) and (14), and then converted to visual angle V by (15):

$$A = \frac{1}{9}\sum_{I=1}^{9}\frac{1}{n}\sum_{j=1}^{n}\left|\left|p_{i,j} - s_i\right|\right| \quad (13)$$

$$P = \frac{}{\frac{1}{9}\sum_{i=1}^{9}\sqrt{\frac{1}{n}\sum_{j=1}^{n}\left[\left(p_{x,i,j} - a_{x,i}\right)^2 + \left(p_{y,i,j} - a_{y,i}\right)^2\right]}} \quad (14)$$

The ith evaluation point (s_i) consists of sample points; p_{ij}($p_{x,i,j}$,$p_{y,i,j}$) is the jth sample point of s_i; $a_{x,i}$ is the mean of abscissas of sample points; and $a_{y,i}$ is the mean of ordinates of sample points [12,13].

$$V = 2arc\tan\left(\frac{0.294K}{2\times 600}\right) \quad (15)$$

Where K is the accuracy (A) or precision (P) of each eye tracker of each subject, resulting in the visual angle A_V and P_V, respectively [12].

b. The validation of filtered and raw data

The ratio of the number of filtered-raw data and the raw-ideal data are calculated.

RESULTS

This section shows the experimental results of the evaluation process, designed in Evaluation section. Table 2 shows the accuracies and precision of the IMR and the VT3 Mini, corresponding to each subject whereas Table 3 indicates the overall accuracy and precision of each device.

DISCUSSION

This section illustrates the experimental analysis of the evaluation process.

Precision and accuracy

Except for N.C.D.test1 and N.C.D.test2, the precision of the commercial eye tracker VT3 Mini eye tracker is better than the proposed device IMR for each subject, and subjects having no sight corrections have better precision than those wearing glasses for each eye tracker. The overall precision of the IMR eye tracker is 0.57 degrees, which nearly equals that of the VT3 Mini device (their ratio is 1.06). This result proves that both devices might have the same ability to reproduce reliably the same their own estimated gaze points.

In contrast, except for H.T.T.D, the accuracy of the IMR is better than those of the VT3 Mini device for each subject. It is also noticed that high deviations between VT3 Mini's gaze points and stimulus points, which appear at the beginning of evaluation duration for each one in nine evaluation points, affect the overall accuracy of this device (as shown in Figure 6 and Figure 7, Appendix section). This phenomenon might be due to the VT3's default smoothing method (Weighted Previous Frame). Regarding the subjects' accuracies of each eye tracker, these values of subjects, having no sight corrections, are better than those of people wearing glasses, expecting for N.C.D.test2 (estimated by the VT3) and N.C.D.test1. According to Table 3, the overall accuracy of the IMR eye tracker is 1.04 degrees which is better than that of the VT3 Mini device (their ratio is 0.78) and is just over the target value (1 degree).

Because the accuracies and precision, evaluated from N.C.D.test1, N.C.D.test2 and H.T.T.D, have striking differences from their groups, their deviations between gaze points and stimulus points over time D are analyzed (consisting of wearing-glass groups, non-wearing-glass groups, IMR's precision groups, VT3's precision groups, IMR's accuracy groups, and VT3's accuracy groups). In Figure 6 and Figure 7, some sample points of these subjects whose D values are greater than 250 pixels (73.5 mm) for N.C.D.test2 and 500 pixels (147 mm) for N.C.D.test1 and H.T.T.D. These results could be affected by the subject's lack of concentration because both eye trackers exhibit high D values at these sample points. However, they might also be affected by the system's lack of stability (hardware or software, or both) because both devices exhibit high precision values.

The validation of filtered and raw data

Regarding the validation of the raw data, the ratios between filtered and recorded samples are shown in Table 4 (see Appendix section), 7 filter samples are lower than 22.5 (half of the ideal sample) at least one in nine evaluation points. It is also noticed that most of these points have the number of raw data of 45, resulting in a high overall ratio between filtered and raw samples (RIR, 98.63%). It is noted that the fifth evaluation point, where subjects' faces are opposite the monitor, has the maximum ratio between filtered and raw samples (FRR) and RIR. Because raw data is obtained in case both devices successfully estimate gaze

Table 2: The accuracy-precision of each device corresponding to each subject

Subject	P of IMR	P of VT3	A of IMR	A of VT3	Glass
T.T.T	13.75	13.17	35.72	38.42	No
D.T.P.test1	16.18	14.58	26.66	37.59	No
D.T.P.test2	15.37	9.39	29.92	36.31	No
D.T.P.test3	12.65	12.44	22.98	36.33	No
D.T.P.test4	12.18	7.55	23.52	35.04	No
N.C.B	14.29	13.67	31.81	34.49	No
N.C.D.test1	**40.62**	**48.55**	**66.54**	**108.47**	No
N.C.D.test2	**17.83**	**24.98**	29.38	**52.71**	No
H.T.T.D	36.97	28.24	**54.95**	**45.04**	Yes
L.Q.T.N	26.05	23.94	50.58	62.15	Yes
V.Q.K	16.81	16.08	37.29	40.45	Yes

Bold numbers indicate that they have striking differences from their groups.

Table 3: The best-mean-worst accuracy and precision of each device correspoding to each subject

Metric		Best	Mean	Worst
IMR	PV	0.34	0.57	1.14
	AV	0.65	1.04	1.87
VT3 Mini	PV	0.21	0.54	1.36
	AV	0.97	1.34	3.04

points (see Evaluation method section), we cannot determine which device significantly loses data. However, the overall FRR (88.92%) is much lower than that of RIR, which significantly is affected by L.Q.T.N. Because filtered points of both devices are collected in which the corresponding raw points are not outside the operating window (see Evaluation method section), we cannot determine which device significantly loses data.

Regarding N.C.D.test1, N.C.D.test2 and H.T.T.D, their FRR and RIR do not have striking differences from their groups. Combining with results from Precision and accuracy section, the accuracy and precision values are affected significantly by the subject's lack of attention.

CONCLUSION

The experimental evaluation in a challenge condition shows that the proposed IMR eye tracker meets technical criteria involving the cost, the eye safety, the sampling frequency, the precision, the accuracy and the validation of raw data. However, it exhibits a failure in the validation of filtered data of certain point(s) for each subject. The IMR device probably is appropriate for the education purpose and needs to be improved to adapt to the research purpose.

ACKNOWLEDGEMENTS

This research is funded by Ho Chi Minh City University of Technology – VNU-HCM under grant number T-KHUD-2020-72.

CONFLICT OF INTEREST

The authors declare that they have no conflict of interest.

AUTHORS' CONTRIBUTION

Phu Do Tuong conceived and designed the IMR system as well as the proposed algorithms, performed the evaluation process, collected the data, and wrote the paper.

Linh Huynh Quang reviewed the eye tracking methodology and pupil detection methods, conceived the data discussion, and reviewed the manuscript.

Dang Le Cao conceived the evaluation procedure and contributed the evaluation tool-VT3 Mini eye tracker, reviewed eye tracking applications regarding

Table 4: The number of filtered and raw samples and their ratios corresponding to each subject. Bold-italic numbers indicate that their values are smaller than 22.5 (the half of the number of the ideal sample). FRR is the ratio between filtered-raw data, and RIR is the ratio of raw-ideal data.

		1	2	3	4	5	6	7	8	9	Average
T.T.T	Filtered data	39	45	40	45	45	45	45	45	45	
	Raw data	44	45	45	45	45	45	45	45	45	
	FRR	88.64	100	88.89	100	100	100	100	100	100	97.5
	RIR	97.78	100	100	100	100	100	100	100	100	99.75
D.T.P.test1	Filtered data	30	45	43	45	45	39	42	39	43	
	Raw data	30	45	45	45	45	40	44	39	43	
	FRR	100	100	95.56	100	100	97.5	95.45	100	100	98.72
	RIR	66.67	100	100	100	100	88.89	97.78	86.67	95.56	92.84
D.T.P.test2	Filtered data	25	45	44	44	45	39	44	45	44	
	Raw data	45	45	45	45	45	45	45	45	44	
	FRR	55.56	100	97.78	97.78	100	86.67	97.78	100	100	92.84
	RIR	100	100	100	100	100	100	100	100	97.78	99.75
D.T.P.test3	Filtered data	44	45	44	45	45	45	45	44	45	
	Raw data	44	45	45	45	45	45	45	45	45	
	FRR	100	100	97.78	100	100	100	100	97.78	100	99.5
	RIR	97.78	100	100	100	100	100	100	100	100	99.75
D.T.P.test4	Filtered data	30	44	45	45	45	45	40	***16***	45	
	Raw data	45	44	45	45	45	45	45	43	45	
	FRR	66.67	100	100	100	100	100	88.89	37.2	100	88.04
	RIR	100	97.78	100	100	100	100	100	95.56	100	99.26
N.C.B	Filtered data	32	***19***	40	44	45	45	42	42	41	
	Raw data	45	45	45	45	45	45	42	45	45	
	FRR	71.11	42.22	88.89	97.78	100	100	100	93.33	91.11	87.16
	RIR	100	100	100	100	100	100	93.33	100	100	99.26
N.C.D.test1	Filtered data	***7***	45	43	45	45	45	44	26	44	
	Raw data	34	45	45	45	45	45	45	42	45	
	FRR	20.59	100	95.56	100	100	100	97.78	61.9	97.78	85.96
	RIR	75.56	100	100	100	100	100	100	93.33	100	96.54
N.C.D.test2	Filtered data	***16***	45	44	45	45	44	44	37	44	
	Raw data	44	45	45	45	45	44	45	45	45	
	FRR	36.36	100	97.78	100	100	100	97.78	82.22	97.78	90.21
	RIR	97.78	100	100	100	100	97.78	100	100	100	99.51
H.T.T.D	Filtered data	37	45	40	45	45	45	3	45	39	
	Raw data	39	45	45	45	45	45	45	45	45	
	FRR	94.87	100	88.89	100	100	100	6.67	100	86.67	86.34
	RIR	86.67	100	100	100	100	100	100	100	100	98.52
L.Q.T.N	Filtered data	***3***	44	***3***	***13***	45	37	42	45	***22***	
	Raw data	45	45	45	45	45	45	45	45	45	
	FRR	6.67	97.78	6.67	28.89	100	82.22	93.33	100	48.89	62.72
	RIR	100	100	100	100	100	100	100	100	100	100
V.Q.K	Filtered data	***10***	45	36	45	45	45	45	45	44	
	Raw data	45	45	45	45	45	45	45	45	44	
	FRR	22.22	100	80	100	100	100	100	100	100	89.14
	RIR	100	100	100	100	100	100	100	100	97.78	99.75
All	FRR										88.92
	RIR										98.63

education-expert training, meditation, and psychology. In the BME laboratory, he is the foundation leader of eye tracking applications.

Tin Tran Trung conceived the scientific idea, reviewed low-cost eye tracking technologies, conceived and designed the IMR system's hardware, reviewed the proposed algorithms, performed the evaluation process, collected the data, and reviewed the manuscript.

REFERENCES

1. Hosp B, et al. RemoteEye: An open-source high-speed remote eye tracker : Implementation insights of a pupil- and glint-detection algorithm for high-speed remote eye tracking," Behav Res Methods. 2020;52(3):1387–1401. PMID: 32212086. Available from: https://doi.org/10.3758/s13428-019-01305-2.
2. Millán YA, et al. A Review on Biometric Devices to be Applied in ASD Interventions. in 2020 Congreso Internacional de Innovación y Tendencias en Ingeniería (CONIITI). 2020;p. 1–6. PMID: 32401697. Available from: https://doi.org/10.1109/CONIITI51147.2020.9240291.
3. Funke G, et al. Which Eye Tracker Is Right for Your Research? Performance Evaluation of Several Cost Variant Eye Trackers," Proceedings of the Human Factors and Ergonomics Society Annual Meeting. 2016;60(1):1240–1244. Available from: https://doi.org/10.1177/1541931213601289.
4. Kim JH, Jeong JW. Gaze in the Dark: Gaze Estimation in a Low-Light Environment with Generative Adversarial Networks. Sensors;20(17):4935–2020. PMID: 32878209. Available from: https://doi.org/10.3390/s20174935.
5. Morimoto CH, Mimica MRM. Eye gaze tracking techniques for interactive applications. Computer Vision and Image Understanding. 2005;98(1):4–24. Available from: https://doi.org/10.1016/j.cviu.2004.07.010.
6. Sheena D, Borah J. Compensation for some second order effects to improve eye position measurements. in Eye Movements: Routledge. 2017;p. 257–268. Available from: https://doi.org/10.4324/9781315437415-21.
7. Manuri F, Sanna A, Petrucci CP. PDIF: Pupil Detection After Isolation and Fitting. IEEE Access. 2020;8:30826–30837. Available from: https://doi.org/10.1109/ACCESS.2020.2973005.
8. Fuhl W, et al. Fast and Robust Eyelid Outline and Aperture Detection in Real-World Scenarios. in 2017 IEEE Winter Conference on Applications of Computer Vision (WACV). 2017;p. 24–31. Available from: 10.1109/WACV.2017.126.
9. Borsato FH, Morimoto CH. Building Structured Lighting Applications Using Low-Cost Cameras. in 2017 30th SIBGRAPI Conference on Graphics, Patterns and Images (SIBGRAPI). 2017;p. 15–20. Available from: https://doi.org/10.1109/SIBGRAPI.2017.9.
10. Świrski L, et al. Robust real-time pupil tracking in highly off-axis images. presented at the Proceedings of the Symposium on Eye Tracking Research and Applications, Santa Barbara, California. [Online]. 2012;Available from: https://doi.org/10.1145/2168556.2168585.
11. To MPS, et al. Vision out of the corner of the eye. Vision Research. 2011;51(1):203–214. Available from: https://doi.org/10.1016/j.visres.2010.11.008.
12. Duchowski AT. Eye Tracking Methodology Theory and Practice, 3rd ed. 2017. ed. Cham: Springer International Publishing. 2017;Available from: https://doi.org/10.1007/978-3-319-57883-5.
13. Blignaut P, Beelders T. The precision of eye-trackers: a case for a new measure. presented at the Proceedings of the Symposium on Eye Tracking Research and Applications, Santa Barbara, California, 2012. [Online];Available from: https://doi.org/10.1145/2168556.2168618.

APPENDIX

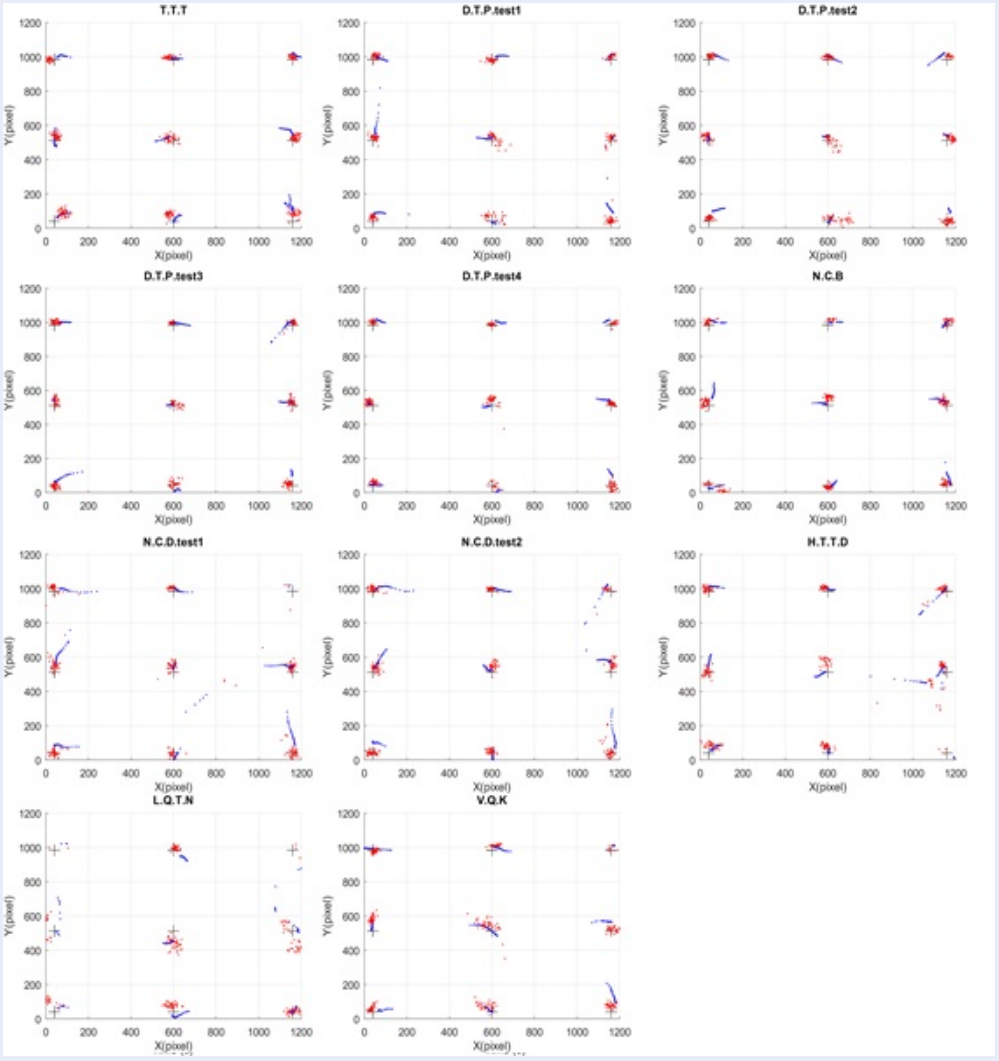

Figure 5: Gaze points of 11 samples are estimated by two eye trackers. Whereas black pluses represent stimulus points, red and blue dots show filtered gaze points of the IMR and VT3 Mini device in the evaluation process, respectively.

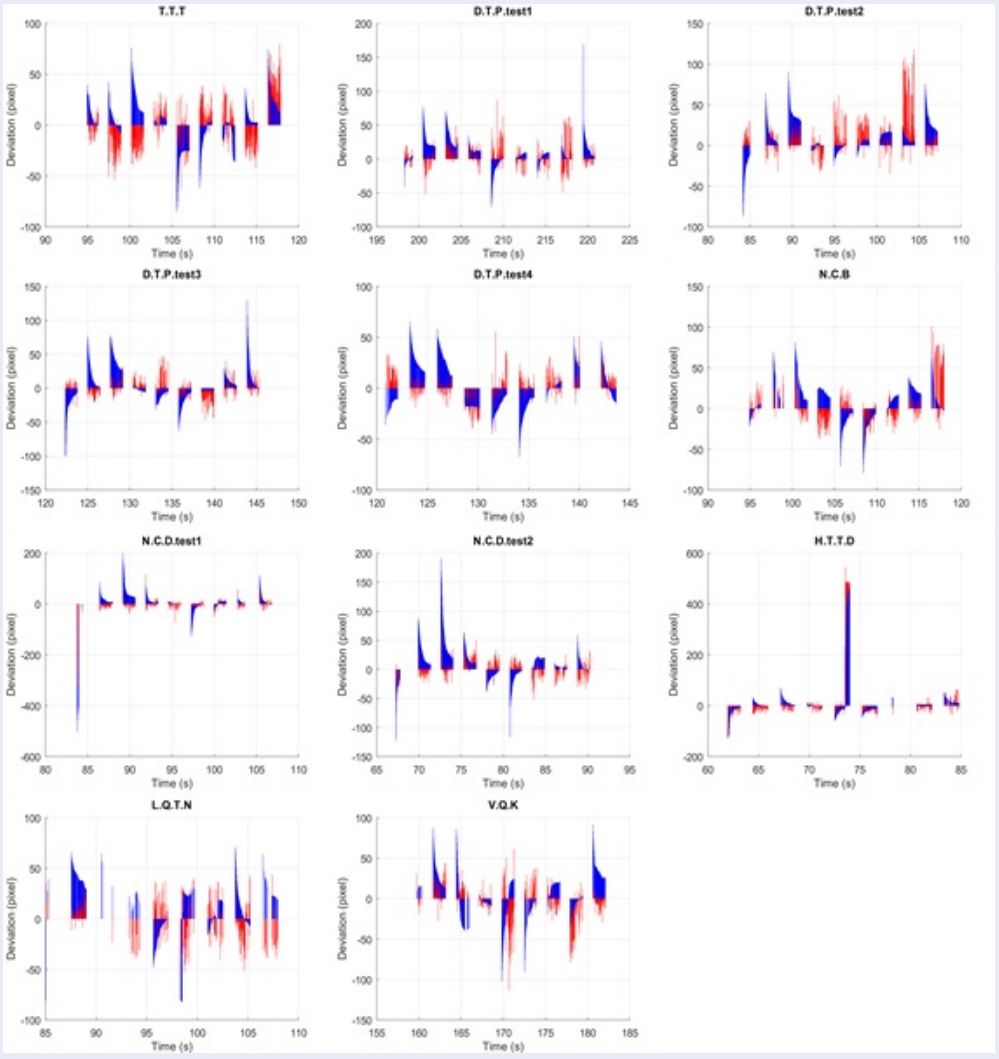

Figure 6: Horizontal deviations between gaze and stimulus points of 11 samples over time, using two eye trackers. Red and blue lines represent the deviations of the IMR and VT3 Mini device, respectively.

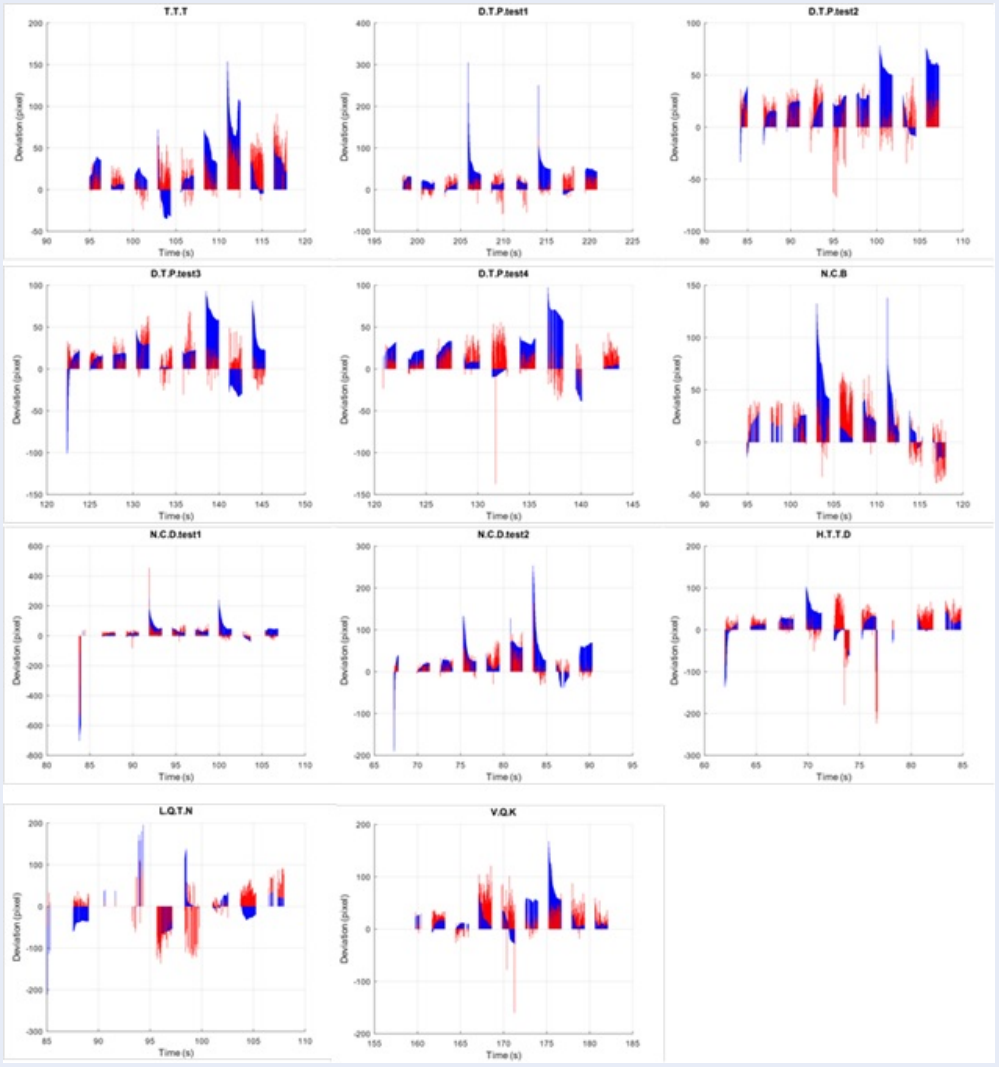

Figure 7: Vertical deviations between gaze and stimulus points of 11 samples over time, using two eye trackers. Red and blue lines represent these deviations of the IMR and VT3 Mini device, respectively.

Tạp chí Phát triển Khoa học và Công nghệ – Kĩ thuật và Công nghệ, 4(3):1079-1092

Open Access Full Text Article

Bài nghiên cứu

Thiết kế thiết bị theo dõi mắt từ xa giá thành thấp, sử dụng kỹ thuật Tâm Đồng Tử-Ảnh Phản Xạ Giác Mạc

Đỗ Tường Phủ, Huỳnh Quang Linh, Lê Cao Đăng, Trần Trung Tín*

Use your smartphone to scan this QR code and download this article

TÓM TẮT

Thiết bị theo dõi mắt được sử dụng trong nhiều lĩnh vực như giáo dục, tiếp thị, tâm lý, y học, vân vân. Tuy nhiên, các thiết bị thương mại khá đắt, trong khoảng từ vài trăm đến vài nghìn USD. Do đó, một thiết bị theo mắt từ xa-giá thành thấp-sử dụng cho một mắt được phát triển cho mục đích giáo dục và nghiên cứu, sử dụng kỹ thuật Tâm Đồng Tử-Ảnh Phản Xạ Giác Mạc (IMR). Thiết bị IMR gồm một camera giá thành thấp nhằm thu nhận ảnh mắt, một máy tính thông thường nhằm xử lý các ảnh này, và hai nguồn sáng hồng ngoại gần nhằm tạo các điểm phản xạ giác mạc và chiếu sáng vùng mắt. Một thuật toán ước lượng tâm đồng tử được phát triển bằng việc kết hợp những ưu điểm của hai thuật gần đây, BORE và PIDF, và điểm nhìn của đối tượng đo được ước lượng từ các vector tâm đồng tử-ảnh phản xạ giác mạc thông qua một đa thức bậc bốn. Việc đánh giá thực nghiệm được tiến hành đồng thời trên thiết bị IMR tại tần số hoạt động 30 Hz và thiết bị thương mại-giá thành cao-cho phép chuyển động đầu tự do VT3 Mini tại tần số 60 Hz, trong điều kiện không lí tưởng: các đối tượng đo ngồi gần một cửa sổ, và một trong số họ có mang kính. Đồng thời, đầu của họ được đặt cố định trên một hệ thống tựa cằm đã được cố định vị trí, và dữ liệu được thu thập khi thiết bị IMR và VT3 Mini lần lượt ước lượng thành công tâm đồng tử-ảnh phản xạ giác mạc và tọa độ điểm nhìn tương ứng. Kết quả thực nghiệm từ 11 dữ liệu của 7 đối tượng đo cho thấy tỷ lệ trung bình số mẫu của của dữ liệu sau và trước khi lọc cũng như tỷ lệ trên đối với số lượng dữ liệu trước khi lọc và số lượng dữ liệu lý tưởng lần lượt là 88,92% và 98,63%. Đồng thời, giá trị precision trung bình của thiết bị IMR gần như tương đương với thiết bị VT3 Mini (lần lượt là 0,57 độ và 0,54 độ) trong khi accuracy trung bình của thiết bị đề xuất tốt hơn thiết bị thương mại (lần lượt là 1,04 độ và 1,34 độ). Về khía cạnh an toàn mắt, công suất bức xạ và độ bức xạ theo trọng số tổn thương do bỏng (burn hazard weighted radiance) nhỏ hơn nhiều so với các giá trị giới hạn tương ứng, theo tiêu chuẩn IEC 62471. Từ những kết quả trên, thiết bị được đề xuất IMR phù hợp với mục tiêu đào tạo và cần được cải tiến về khía cạnh tỷ lệ mẫu được ước lượng thành công nhằm đạt mục tiêu nghiên cứu.

Từ khoá: Thiết bị theo dõi mắt, ước lượng điểm nhìn, giá thành thấp, kỹ thuật Tâm Đồng Tử-Ảnh Phản Xạ Giác Mạc, phát hiện tâm đồng tử

Ngành Kỹ Thuật Y Sinh, Khoa Khoa học Ứng dụng, Trường Đại học Bách Khoa, ĐHQG-HCM, Việt Nam

Liên hệ

Trần Trung Tín, Ngành Kỹ Thuật Y Sinh, Khoa Khoa học Ứng dụng, Trường Đại học Bách Khoa, ĐHQG-HCM, Việt Nam

Email: trtrtin@hcmut.edu.vn

Lịch sử

- Ngày nhận: 03-06-2021
- Ngày chấp nhận: 30-8-2021
- Ngày đăng: 11-9-2021

DOI : 10.32508/stdjet.v4i3.856

Check for updates

VNU-HCM Press

Trích dẫn bài báo này: Phủ D T, Linh H Q, Đăng L C, Tín T T. **Thiết kế thiết bị theo dõi mắt từ xa giá thành thấp, sử dụng kỹ thuật Tâm Đồng Tử-Ảnh Phản Xạ Giác Mạc**. *Sci. Tech. Dev. J. - Eng. Tech.;* 4(3):1079-1092.